Inorg. Chem. **2007**, *46*, 8684–8689

Magnetic Properties of Synthetic Libethenite Cu_2PO_4OH: a New Spin-Gap System

Alexei A. Belik,*[†,‡] Hyun-Joo Koo,[§] Myung-Hwan Whangbo,[∥] Naohito Tsujii,[⊥] Panče Naumov,[‡] and Eiji Takayama-Muromachi[†]

Advanced Nano Materials Laboratory (ANML), International Center for Young Scientists (ICYS), and Quantum Beam Center, National Institute for Materials Science (NIMS), Namiki 1-1, Tsukuba, Ibaraki 305-0044, Japan, Department of Chemistry and Research Institute of Basic Science, Kyung Hee University, Seoul 130-701, South Korea, and Department of Chemistry, North Carolina State University, Raleigh, North Carolina 27695-8204

Received May 2, 2007

Synthetic mineral libethenite Cu_2PO_4OH was prepared by the hydrothermal method, and its structure at 200 K was refined by single-crystal X-ray diffraction. The structure of Cu_2PO_4OH is built up from $Cu2_2O_6(OH)_2$ dimers of edge-sharing $Cu2O_4(OH)$ trigonal bipyramids and $[Cu1_2O_6(OH)_2]_\infty$ chains of edge-sharing $Cu1O_4(OH)_2$ octahedra. Magnetic properties of Cu_2PO_4OH were investigated by magnetic susceptibility, magnetization, and specific heat measurements. Cu_2PO_4OH is a spin-gap system with a spin gap of about 139 K. It was shown by spin dimer analysis that, to a first approximation, the magnetic structure of Cu_2PO_4OH is described by an isolated square-spin cluster model defined by the Cu1–O–Cu2 superexchange J with Cu1···Cu2 = 3.429 Å. The fitting analysis of the magnetic susceptibility data with a square-spin cluster model results in $J/k_B = 138$ K. Specific heat data show that Cu_2PO_4OH does not undergo a long-range magnetic ordering down to 1.8 K. We also report vibrational properties studied with Raman spectroscopy and the thermal stability of Cu_2PO_4OH.

1. Introduction

Low-dimensional quantum magnets have attracted considerable attention because of interesting physical properties. Many low-dimensional magnetic systems with a spin-singlet ground state have been discovered,[1−3] e.g., the $S = {}^1/_2$ alternating chain systems $(VO)_2P_2O_7$,[4] $Na_2Cu_2TeO_6$,[5] and $AgCuPO_4$,[6] the $S = {}^1/_2$ two-leg ladder systems $SrCu_2O_3$ and $Sr_{14}Cu_{24}O_{41}$,[7,8] the $S = 1$ chain (Haldane) systems Y_2BaNiO_5 and $PbNi_2V_2O_8$,[9,10] the spin-Peierls compound $CuGeO_3$,[11] spin-dimer systems (e.g., $CaCuGe_2O_6$),[12] and linear four-spin cluster systems (e.g., Cu_2PO_4[13] and $SrCu_2(PO_4)_2$).[14] The spin-singlet state is a spin configuration in which the projection of their total moment on any direction is equal to zero, thereby resulting in nonmagnetic behavior at rather low temperatures.[3] The spin-singlet state is separated from the excited triplet state by a spin gap. The magnetic systems of Cu^{2+} ions are particularly interesting because the quantum effect is strong for spin-${}^1/_2$ systems because they have large quantum fluctuations.

* To whom correspondence should be addressed. E-mail: alexei.belik@nims.go.jp.
[†] ANML, NIMS.
[‡] ICYS, NIMS.
[§] Kyung Hee University.
[∥] North Carolina State University.
[⊥] Quantum Beam Center, NIMS.

(1) Johnston, D. C.; Kremer, R. K.; Troyer, M.; Wang, X.; Klümper, A.; Bud'ko, S. L.; Panchula, A. F.; Canfield, P. C. *Phys. Rev. B* **2000**, *61*, 9558.
(2) Ueda, Y. *Chem. Mater.* **1998**, *10*, 2653.
(3) Vasil'ev, A. N.; Markina, M. M.; Popova, E. A. *Low Temp. Phys.* **2005**, *31*, 203.
(4) (a) Azuma, M.; Saito, T.; Fujishiro, Y.; Hiroi, Z.; Takano, M.; Izumi, F.; Kamiyama, T.; Ikeda, T.; Narumi, Y.; Kindo, K. *Phys. Rev. B* **1999**, *60*, 10145. (b) Koo, H.-J.; Whangbo, M.-H.; VerNooy, P. D.; Torardi, C. C.; Marshall, W. J. *Inorg. Chem.* **2002**, *41*, 4664.
(5) Xu, J. X.; Assoud, A.; Soheilnia, N.; Derakhshan, S.; Cuthbert, H. L.; Greedan, J. E.; Whangbo, M. H.; Kleinke, H. *Inorg. Chem.* **2005**, *44*, 5042.
(6) Ben Yahia, H.; Gaudin, E.; Darriet, J.; Dai, D.; Whangbo, M. H. *Inorg. Chem.* **2006**, *45*, 5501.
(7) Azuma, M.; Hiroi, Z.; Takano, M.; Ishida, K.; Kitaoka, Y. *Phys. Rev. Lett.* **1994**, *73*, 3463.
(8) Eccleston, R. S.; Uehara, M.; Akimitsu, J.; Eisaki, H.; Motoyama, N.; Uchida, S. I. *Phys. Rev. Lett.* **1998**, *81*, 1702.
(9) Darriet, J.; Regnault, L. P. *Solid State Commun.* **1993**, *86*, 409.
(10) Uchiyama, Y.; Sasago, Y.; Tsukada, I.; Uchinokura, K.; Zheludev, A.; Hayashi, T.; Miura, N.; Böni, P. *Phys. Rev. Lett.* **1999**, *83*, 632.
(11) Hase, M.; Terasaki, I.; Uchinokura, K. *Phys. Rev. Lett.* **1993**, *70*, 3651.
(12) Valentí, R.; Saha-Dasgupta, T.; Gros, C. *Phys. Rev. B* **2002**, *66*, 054426.
(13) Hase, M.; Etheredge, K. M. S.; Hwu, S.-J.; Hirota, K.; Shirane, G. *Phys. Rev. B* **1997**, *56*, 3231.
(14) Belik, A. A.; Azuma, M.; Matsuo, A.; Whangbo, M. H.; Koo, H. J.; Kikuchi, J.; Kaji, T.; Okubo, S.; Ohta, H.; Kindo, K.; Takano, M. *Inorg. Chem.* **2005**, *44*, 6632.

10.1021/ic7008418 CCC: $37.00
Published on Web 09/12/2007

Recently, magnetic properties of some Cu-containing minerals have been intensively studied because of the peculiar crystal structures and magnetic ion sublattices, for example, azurite $Cu_3(CO_3)_2(OH)_2$[15] and clinoatacamite $Cu_2Cl(OH)_3$.[16] The Cu−P−O and Cu−P−O−H systems show rich crystal chemistry and hence variations in magnetic sublattices. So far about 15 structures in the Cu−P−O and Cu−P−O−H systems have been reported.[17] Mineral libethenite Cu_2PO_4OH was discovered in 1823.[18] Various physical and chemical properties, for example, the morphological,[17] structural,[19−21] optical,[18] vibrational,[22−25] and catalytic properties,[26,27] of natural and synthetic libethenite have been investigated. Surprisingly, however, detailed magnetic properties of Cu_2PO_4OH have not been investigated yet. To the best of our knowledge, only one paper reported magnetic susceptibilities of Cu_2PO_4OH without appropriate discussion.[28] The compounds Co_2PO_4OH[29−31] and Co_2AsO_4OH,[32] which are isotructural with Cu_2PO_4OH, demonstrate interesting magnetic properties. For example, Co_2PO_4OH exhibits spin-glass behavior in a three-dimensional antiferromagnet ordered phase.[29]

In this work, we have investigated magnetic properties of synthetic libethenite Cu_2PO_4OH by magnetic susceptibility, isothermal magnetization (up to 300 kOe), and specific heat measurements as well as by spin dimer analysis. Although the crystal structure of Cu_2PO_4OH consists of the structural dimers $Cu2_2O_6(OH)_2$ with Cu2···Cu2 = 3.057 Å and one-dimensional (1D) $[Cu1_2O_6(OH)_2]_\infty$ chains, the magnetic properties of Cu_2PO_4OH are described by a square-spin cluster (SQSC) model whose spin-exchange paths do not include the structural dimer. We have also studied the thermal stability and vibrational properties of Cu_2PO_4OH by Raman spectroscopy.

2. Experimental Section

Synthesis. Initially, single crystals of Cu_2PO_4OH were obtained by the hydrothermal method during an attempt to grow single crystals of an almost ideal 1D Heisenberg antiferromagnet $Sr_2Cu(PO_4)_2$.[33,34] $Cu(NO_3)_2{\cdot}3H_2O$ (0.7470 g) and $Sr(NO_3)_2$ (1.3088 g) were dissolved in distilled water, and then a water solution of $NH_4H_2PO_4$ (0.7113 g) was added (the mole ratio Sr:Cu:PO_4 = 2:1:2). The water volume was adjusted to 20 mL. The solution with blue sediment was placed in a Teflon capsule having a volume of 50 mL. A stainless steel autoclave with the Teflon capsule was heated up to 473 K during 20 h and kept it for 50 h, and then the temperature was decreased to 350 K for 50 h. In another synthesis, we mixed water solutions of $Cu(NO_3)_2{\cdot}3H_2O$ (1.8882 g) and $NH_4H_2PO_4$ (0.4493 g) (the mole ratio Cu:PO_4 = 2:1), adjusted the water volume to 20 mL in the Teflon capsule, heated the capsule up to 473 K for 4 h, kept it for 150 h, and decreased the temperature to 350 K for 120 h. After these procedures, green single crystals of Cu_2PO_4OH were obtained (see the Supporting Information). Powder X-ray diffraction (XRD) data of the crushed single crystals showed that the samples were single-phased (see the Supporting Information).

Single-Crystal XRD and Structure Refinement. Single-crystal XRD data were collected in ω-oscillation mode with a Bruker three-circle diffractometer equipped with a CCD detector and a helium−dinitrogen open-type low-temperature system, using graphite-monochromatized Mo Kα X-ray radiation (0.710 73 Å, 40 kV, 40 mA). A total of 1300 frames of 0.3° width were collected by a 45 s exposure of an emerald-green single crystal measuring 200 × 180 × 175 μm that has been flash-frozen and kept at a nominal temperature of 200 K (uncorrected). The merge and integration yielded 6722 reflections (617 unique after the merge; limiting indices, $-11 \leftarrow h \leftarrow 11$, $-11 \leftarrow k \leftarrow 11$, $-8 \leftarrow l \leftarrow 4$, of which 460 were rejected with the $2\Theta_{max}$ cutoff criterion of 60°, giving a factor of internal consistency R_{int} = 3.96%). The crystals are orthorhombic, space group *Pnnm*, with unit cell parameters a = 8.0513(9) Å, b = 8.3775(10) Å, c = 5.8799(7) Å, $\alpha = \beta = \gamma$ = 90°, V = 396.60(8) Å^3, Z = 4, ρ_{calc} = 4.004 g·cm^{-3}, $F(000)$ = 456 (μ = 11.028 mm^{-1}). The lattice parameters are close to those reported in the literature for mineral and synthetic libethenite (a = 8.06−8.08 Å, b = 8.38−8.43 Å, and c = 5.88−5.90 Å at room temperature).[18−20] The very small difference is due to the lower temperature. The structure was solved with direct methods,[35] and 48 parameters were refined on F^2 using 617 reflections,[36] assigning anisotropic displacement parameters to all non-hydrogen atoms. The hydrogen atom was located in the difference Fourier map at 0.95 Å from O4 and included in the final round of refinement without constraints. The final agreement factors were R_1 = 3.81% (wR_2 = 10.11%) for 577 reflections with $I > 2\sigma(I)$ and R_1 = 3.97% (wR_2 = 10.18%) for all 617 reflections; GOF = 1.306. The highest peak and hole of +0.98 and −2.66 e·Å^{-3} in the final difference Fourier were located 1.71 Å from O1 and 0.06 Å from Cu1. The

(15) Kikuchi, H.; Fujii, Y.; Chiba, M.; Mitsudo, S.; Idehara, T.; Tonegawa, T.; Okamoto, K.; Sakai, T.; Kuwai, T.; Ohta, H. *Phys. Rev. Lett.* **2005**, *94*, 227201.
(16) Zheng, X. G.; Kubozono, H.; Nishiyama, K.; Higemoto, W.; Kawae, T.; Koda, A.; Xu, C. N. *Phys. Rev. Lett.* **2005**, *95*, 057201.
(17) Xu, J.; Xue, D. *J. Phys. Chem. B* **2006**, *110*, 7750.
(18) (a) http://euromin.w3sites.net/mineraux/LIBETHENITE.html. (b) http://www.mindat.org/min-2394.html.
(19) Yakubovich, O. V.; Melnikov, O. K. *Kristallografiya* **1993**, *38*, 63.
(20) (a) Cordsen, A. *Can. Miner.* **1978**, *16*, 153. (b) Heritsch, H. *Z. Kristallogr.* **1940**, *102*, 1. (c) Keller, P.; Hess, H.; Zettler, F. *Neues Jahrb. Mineral., Abh.* **1979**, *134*, 147.
(21) Braithwaite, R. S. W.; Pritchard, R. G.; Paar, W. H.; Pattrick, R. A. D. *Mineral. Mag.* **2005**, *69*, 145.
(22) Reddy, N. C. G.; Reddy, R. R.; Reddy, G. S.; Reddy, S. L.; Reddy, B. J. *Cryst. Res. Technol.* **2006**, *41*, 400.
(23) Martens, W.; Frost, R. L. *Am. Mineral.* **2003**, *88*, 37.
(24) Frost, R. L.; Williams, P. A.; Martens, W.; Kloprogge, J. T.; Leverett, P. *J. Raman Spectrosc.* **2002**, *33*, 260.
(25) *The Infrared Spectra of Minerals*; Farmer, V. C., Ed.; Mineralogical Society Monograph 4; Mineralogical Society: London, 1974; p 397.
(26) Xiao, F. S.; Sun, J. M.; Meng, X. J.; Yu, R. B.; Yuan, H. M.; Xu, J. N.; Song, T. Y.; Jiang, D. Z.; Xu, R. R. *J. Catal.* **2001**, *199*, 273.
(27) Meng, X. J.; Lin, K. F.; Yang, X. Y.; Sun, Z. H.; Jiang, D. Z.; Xiao, F. S. *J. Catal.* **2003**, *218*, 460.
(28) de Pedro, I.; Jubera, V.; Rojo, J. M.; Lezama, L.; Sanchez Marcos, J.; Rodríguez Fernández, J.; Mesa, J. L.; Rojo, T.; Arriortua, M. I. *J. Magn. Magn. Mater.* **2004**, *272−276*, E665.
(29) Rojo, J. M.; Mesa, J. L.; Lezama, L.; Pizarro, J. L.; Arriortua, M. I.; Fernandez, J. R.; Barberis, G. E.; Rojo, T. *Phys. Rev. B* **2002**, *66*, 094406.
(30) de Pedro, I.; Rojo, J. M.; Jubera, V.; Fernandez, J. R.; Marcos, J. S.; Lezama, L.; Rojo, T. *J. Mater. Chem.* **2004**, *14*, 1157.
(31) de Pedro, I.; Rojo, J. M.; Pizarro, J. L.; Fernandez, J. R.; Marcos, J. S.; Fernandez-Diaz, M. T.; Arriortua, M. I.; Rojo, T. *J. Phys.: Condens. Matter* **2006**, *18*, 3767.
(32) Rojo, J. M.; Mesa, J. L.; Lezama, L.; Barberis, G. E.; Rojo, T. *J. Magn. Magn. Mater.* **1996**, *158*, 493.
(33) Belik, A. A.; Uji, S.; Terashima, T.; Takayama-Muromachi, E. *J. Solid State Chem.* **2005**, *178*, 3461.
(34) Johannes, M. D.; Richter, J.; Drechsler, S.-L.; Rosner, H. *Phys. Rev. B* **2006**, *74*, 174435.
(35) Altomare, A.; Cascarano, G.; Giacovazzo, C.; Guagliardi, A.; Burla, M. C.; Polidori, G.; Camalli, M. *J. Appl. Crystallogr.* **1994**, *27*, 435.
(36) Sheldrick, G. M. E. *SHELXL-97: Structure refinement program*; University of Göttingen: Göttingen, Germany, 1997.

Table 1. Fractional Coordinates and Atomic Displacement Parameters (Isotropic for Hydrogen and Equivalent for Non-Hydrogen Atoms, Which Were Refined Anisotropically) of Cu_2PO_4OH at 200 K

atom	Wyckoff position	*x*	*y*	*z*	*U* (Å^2)
Cu1	4*f*	0	0.5	0.24911(9)	0.0061(2)
Cu2	4*g*	−0.36181(7)	0.37495(7)	0.5	0.0077(2)
P	4*g*	−0.23298(14)	0.25163(13)	0	0.0036(3)
O1	4*g*	−0.1331(4)	0.4120(4)	0	0.0054(7)
O2	8*h*	−0.3413(3)	0.2389(3)	0.2106(4)	0.0098(5)
O3	4*g*	−0.1029(5)	0.1159(4)	0	0.0137(8)
O4	4*g*	−0.1236(4)	0.3974(4)	0.5	0.0049(6)
H	4*g*	−0.096(10)	0.289(9)	0.5	0.020(19)

final structure parameters are reported in Table 1, and other details can be found in the Supporting Information. The atomic coordinates obtained in this work are very close to those reported in the literature for the synthetic[19] and mineral[20a] libethenite at room temperature. For the careful spin dimer analysis, the structural data at low temperature are desirable. Therefore, we used our structural parameters determined at 200 K.

Physical and Chemical Characterization. Magnetic susceptibilities, $\chi = M/H$, of a large number of Cu_2PO_4OH single crystals (102.45 mg) were measured on a direct-current SQUID magnetometer (Quantum Design MPMS) between 1.8 and 300 K in applied fields of 1 and 10 kOe under both zero-field-cooled (ZFC) and field-cooled (FC) conditions. Isothermal magnetization curves of Cu_2PO_4OH were recorded at 1.7 K between 0 and 300 kOe using a hybrid magnet of NIMS and at 1.8 and 4.2 K between 0 and 70 kOe using an MPMS.

The specific heat, $C_p(T)$, of Cu_2PO_4OH was measured from 100 to 1.8 K at zero magnetic field and from 20 to 1.8 K at 70 kOe by a pulse relaxation method using a commercial calorimeter (Quantum Design PPMS). In the measurement, we used one single crystal weighing 3.14 mg.

Unpolarized Raman spectra of Cu_2PO_4OH single crystals were collected at room temperature with a micro Raman spectrometer (Horiba Jobin-Yvon T64000) in backscattering geometry with a liquid-nitrogen-cooled CCD detector. Raman scattering was excited using an Ar^+-Kr^+ laser at a wavelength of 514.5 nm. A 90× long working distance objective was used to focus the laser beam onto a spot of about 2 μm in diameter. The laser power on the samples was about 2 mW.

The Raman spectrum of Cu_2PO_4OH consists of a sharp peak at 3475 cm^{-1} due to the hydroxyl stretching vibration, a sharp peak at 815 cm^{-1} due to the hydroxyl bending vibration,[23] and other Raman bands distributed in four wavenumber ranges: 50−350, 380−500, 500−700, and 870−1200 cm^{-1} (see the Supporting Information). The first range corresponds to the lattice vibrations. The other ranges correspond to the internal modes ν_2, ν_4, ν_1, and ν_3 of a free PO_4^{3-} ion, respectively. For a free PO_4^{3-} tetrahedron, $\nu_1 = 938$ cm^{-1} (symmetric P−O stretching mode of A_1 symmetry), $\nu_2 = 420$ cm^{-1} (O−P−O bending mode of E symmetry), $\nu_3 = 1017$ cm^{-1} (asymmetric P−O stretching mode of T_2 symmetry), and $\nu_4 = 567$ cm^{-1} (O−P−O bending mode of T_2 symmetry).[37] Group analysis of the internal stretching and bending modes of PO_4^{3-} groups in Cu_2PO_4OH predicts the following Raman active modes: $A_g + B_{1g}$ for ν_1, $A_g + B_{1g} + B_{2g} + B_{3g}$ for ν_2, and $2A_g + B_{1g} + B_{2g} + 2B_{3g}$ for ν_3 and ν_4 (total of 18).[38] The experimentally observed bands are 975 cm^{-1} for ν_1; 374, 389, and 455 cm^{-1} for ν_2; 1010, 1019, 1050, 1068, and 1125 cm^{-1} for ν_3; and 557, 585, 593, 626, and 646 cm^{-1} for ν_4 (total of 14). In general, the Raman spectrum of synthetic libethenite is very close to that of minerals,[22−25] but we resolved a few new Raman bands (e.g., at 374, 593, 1010, and 1068 cm^{-1}). The band at 862 cm^{-1} observed in a mineral sample[24] was not detected.

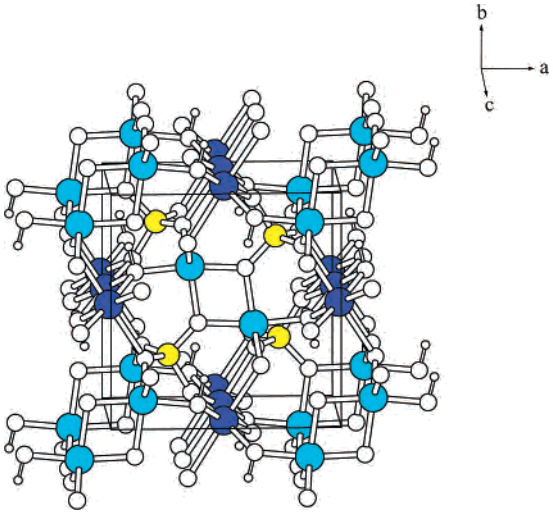

Figure 1. Perspective view of the crystal structure of Cu_2PO_4OH. The blue, cyan, yellow, large white, and small white circles represent Cu1, Cu2, P, O, and H atoms, respectively.

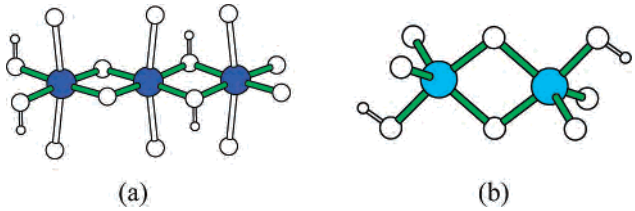

Figure 2. (a) Perspective view of an edge-sharing $[Cu1_2O_6(OH)_2]_\infty$ chain along the *c* axis. (b) Perspective view of an edge-sharing $Cu2_2O_6(OH)_2$ dimer. The Cu−O bonds in green indicate that the magnetic orbitals of the $Cu1^{2+}$ and $Cu2^{2+}$ sites have orbital contributions in these bonds (see Figure 3).

The thermal stability of Cu_2PO_4OH was examined in air with a MacScience TG-DTA 2000 instrument. The sample was placed in a platinum crucible, heated up to 973 K, and then cooled at a rate of 10 K·min^{-1}. Differential thermal analysis (DTA) data showed one exothermal peak centered at 881 K. The weight loss starts from 823 K and reaches 3.70% at 973 K (see the Supporting Information), which is in good agreement with the theoretical loss ($0.5H_2O$) of 3.77%. The temperature stability of Cu_2PO_4OH in air is about 100 K lower than the previously reported value of 923 K.[26,27]

3. Results and Discussion

3.1. Spin Dimer Analysis of Cu_2PO_4OH. There are two different Cu sites in Cu_2PO_4OH (Figure 1). Each Cu1 atom forms an axially elongated $Cu1O_4(OH)_2$ octahedron, and the $Cu1O_4(OH)_2$ octahedra share their short edges [Cu1−O = 2.386 (×2), 1.959 (×2), 1.976 (× 2) Å] to form the $[Cu1_2O_6(OH)_2]_\infty$ chains along the *c* axis (Figure 2a). Each Cu2 atom forms a distorted trigonal bipyramid $Cu2O_4(OH)$ (Cu2−O = 2.055 (× 2), 2.039, 1.943 and 1.922 Å), and each $Cu2_2O_6(OH)_2$ dimer is formed from two trigonal bipyramids by sharing an edge (Figure 2b). Figure 3 depicts the magnetic orbitals of the $Cu1O_4(OH)_2$ octahedron and the $Cu2O_4(OH)$

(37) de Aza, P. N.; Santos, C.; Pazo, A.; de Aza, S.; Cusco, R.; Artus, L. *Chem. Mater.* **1997**, *9*, 912.

(38) Rousseau, D. L.; Bauman, R. P.; Porto, S. P. S. *J. Raman Spectrosc.* **1981**, *10*, 253.

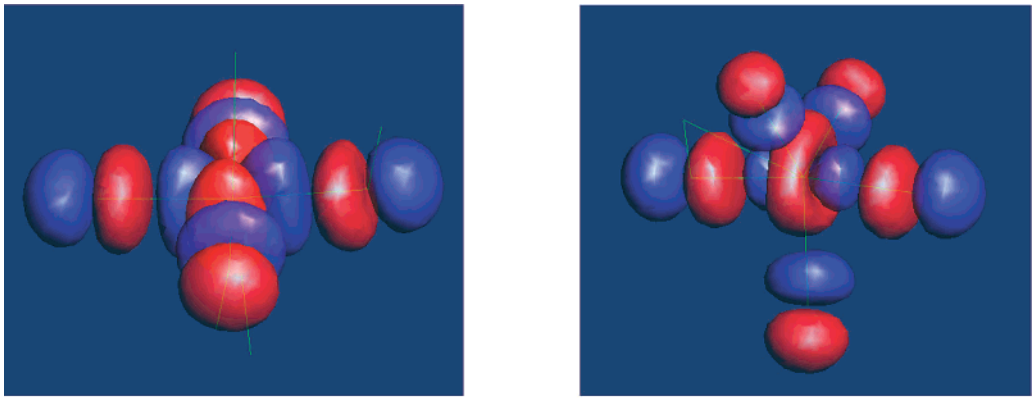

(a) (b)

Figure 3. Magnetic orbitals of (a) the $Cu1O_4(OH)_2$ octahedron and (b) the $Cu2O_4(OH)$ trigonal bipyramid.

trigonal bipyramid obtained from extended Hückel tight-binding (EHTB) calculations.[39−41] The magnetic orbital of the $Cu1O_4(OH)_2$ octahedron has contributions only from the four short Cu1−O bonds (i.e., the "$x^2 - y^2$" orbital with the local x and y axes taken along the short Cu1−O bonds). However, the magnetic orbital of the $Cu2O_4(OH)$ trigonal bipyramid has contributions from all five Cu2−O bonds (i.e., the "z^2" orbital with the local z axis along the two short Cu2−O bonds).

The spin-exchange interactions between the Cu^{2+} ions of Cu_2PO_4OH can occur through the Cu−O−Cu superexchange (SE) and the Cu−O···O−Cu super-superexchange (SSE) paths. It is known that SSE interactions can be rather strong in magnitude, e.g., $J/k_B = 143$ K in $Sr_2Cu(PO_4)_2$,[33,39] and can be even stronger than SE interactions,[40,41] e.g., in edge-sharing 1D chains.[42] To find a spin−lattice model appropriate for analyzing the magnetic susceptibility data of Cu_2PO_4OH, therefore, it is necessary to examine the relative strengths of the SE and SSE interactions. In this section, we estimate these interactions in terms of spin dimer analysis based on EHTB calculations.[40,41]

The geometrical parameters associated with the various SSE paths of Cu_2PO_4OH are listed in Table 2, and the $(\Delta e)^2$ values calculated for the SE and SSE paths with and without the PO_4 units attached to the spin dimers are summarized in Table 3. We considered only the SSE paths connected by PO_4 bridges because other SSE paths have O···O contacts longer than the sum of the van der Waals radii. One exception is the next-nearest-neighbor interaction within the $[Cu1_2O_6(OH)_2]_\infty$ chain, for which Cu1···Cu1 = 5.880 Å and the O···O contacts are not provided by PO_4 bridges. The SE interaction of the $[Cu1_2O_6(OH)_2]_\infty$ chain is negligible, in agreement with the empirical observation that this interaction changes sign and can be almost zero if the Cu−O−Cu bond angle is near 95°.[42] In Cu_2PO_4OH, the Cu1−O−Cu1 bond angles are about 96.7°. However, we note that the empirical rule was obtained for edge-sharing Cu−O chains without OH groups. The SE interaction of the $Cu2_2O_6(OH)_2$ dimer unit is also weak. The strongest SE interaction (J_1) occurs between the Cu1 and Cu2 atoms mediated by the OH group (Figure 4a). This SE is strong because its Cu1−O−Cu2 linkage has short Cu1−O and O−Cu2 bonds (1.976 and 1.927 Å, respectively) and a large ∠Cu1−O−Cu2 angle (122.9°). The next-strongest interaction is the SSE interaction (J_2) between the Cu2 atoms (Figure 4b). The J_1 interactions form isolated square tetramer units Cu1−Cu2−Cu1−Cu2 (Figure 5a), and these SQSCs are weakly interacting through the J_2 interactions (Figure 5b). To a first approximation, therefore, the magnetic lattice of Cu_2PO_4OH may be described by a SQSC model with one spin-exchange parameter $J_1 = J$, i.e., by the spin Hamiltonian

$$\hat{H} = J(\hat{S}_1 \cdot \hat{S}_2 + \hat{S}_2 \cdot \hat{S}_3 + \hat{S}_3 \cdot \hat{S}_4 + \hat{S}_4 \cdot \hat{S}_1) \qquad (1)$$

Table 2. Geometrical Parameters of the SE (a) and SSE (b) Paths in $Cu_2PO_4(OH)$

(a) SE

	Cu···Cu (Å)	Cu−O (Å)	∠Cu−O−Cu (deg)
Cu1/Cu1	2.930	1.959, 1.959	96.8, 96.8
	2.950	1.976, 1.976	96.6, 96.6
Cu2/Cu2	3.056	1.943, 2.038	100.3, 100.3
Cu1/Cu2	3.492	1.927, 1.976	122.9
	3.640	2.055, 2.386	109.9

(b) SSE

	Cu···Cu (Å)	Cu−O (Å)	O···O (Å)	∠Cu−O···O (deg)
Cu1/Cu1	5.880	1.959, 1.976	2.943, 2.943	137.8, 138.4
	5.810	2.386, 1.959	2.539	151.8, 102.2
		2.386, 1.976	2.780	132.6, 93.9
	6.511	2.386, 1.959	2.539	151.8, 160.2
Cu2/Cu2	5.407	2.055, 1.943	2.506	134.3, 138.5
		1.927, 2.055	2.829	139.5, 121.5
	5.425	2.038, 2.055	2.506	107.5, 134.3
Cu1/Cu2	5.448	1.943, 2.386	2.506	138.5, 96.6
		1.943, 1.976	2.864	142.5, 96.3
	5.550	2.038, 1.959	2.492	166.4, 108.7
		2.038, 2.386	2.968	120.3, 84.7

3.2. Magnetic Properties of Cu_2PO_4OH. Figure 6 presents plots of χ and χ^{-1} (ZFC curves) against temperature, T, for Cu_2PO_4OH measured at 10 kOe. No noticeable

(39) Koo, H.-J.; Dai, D.; Whangbo, M.-H. *Inorg. Chem.* **2005**, *44*, 4359.
(40) Whangbo, M.-H.; Dai, D.; Koo, H.-J. *Solid State Sci.* **2005**, *7*, 827.
(41) Whangbo, M.-H.; Koo, H.-J.; Dai, D. *J. Solid State Chem.* **2003**, *176*, 417.
(42) Mizuno, Y.; Tohyama, T.; Maekawa, S.; Osafune, T.; Motoyama, N.; Eisaki, H.; Uchida, S. *Phys. Rev. B* **1998**, *57*, 5326.

Table 3. $(\Delta e)^2$ Values of the SE (a) and SSE (b) Interactions in $Cu_2PO_4(OH)$ Calculated with and without the PO_4 Units Associated with the Spin Dimers[a]

(a) SE

Cu···Cu (Å)	$(\Delta e)^2$ without	$(\Delta e)^2$ with
	Cu1···Cu1	
2.930	500 (0.01)	60 (0.00)
2.950	60 (0.00)	60 (0.00)
	Cu2···Cu2	
3.056	3870 (0.08)	6910 (0.19)
	Cu1···Cu2	
3.429	51100 (1.00)	36200 (1.00)
3.640	350 (0.01)	360 (0.01)

(b) SSE

Cu···Cu (Å)	$(\Delta e)^2$ without	$(\Delta e)^2$ with
	Cu1···Cu1	
5.880	5720 (0.11)	5720 (0.16)[b]
5.810	30 (0.00)	770 (0.02)
6.511	2300 (0.05)	980 (0.03)
	Cu2···Cu2	
5.407	12400 (0.24)	7470 (0.21)
5.425	350 (0.01)	410 (0.01)
	Cu1···Cu2	
5.448	1200 (0.02)	150 (0.00)
5.550	1100 (0.02)	80 (0.00)

[a] The $(\Delta e)^2$ values are in units of $(meV)^2$, and their relative values with respect to the largest value are in parentheses. [b] The O···O contacts of this SSE path are not provided by PO_4 bridges.

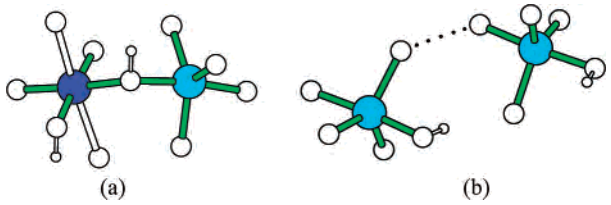

Figure 4. Spin dimers associated with (a) the SE path J_1 and (b) the SSE path J_2.

difference was found between the curves measured under the ZFC and FC conditions and at different magnetic fields. The high-temperature region (250−300 K) was fitted very well by the Curie−Weiss law

$$\chi^{-1}(T) = 3k_B(T - \theta)/(\mu_{eff}{}^2 N) \quad (2)$$

where μ_{eff} (=1.95 μ_B) is the effective magnetic moment that is typical of Cu^{2+} ion, N is Avogadro's number, k_B is Boltzmann's constant, and θ (=−128 K) is the Weiss constant. The negative Weiss constant suggests dominant antiferromagnetic interaction between Cu^{2+} ions.

Below about 150 K, the deviation from the Curie−Weiss law was observed with a broad maxima on the $\chi(T)$ curve at T_M = 110 K, which is typical for low-dimensional Heisenberg antiferromagnets, where T_M is the position of the broad maxima. Below T_M, the magnetic susceptibility decreases rapidly, which is characteristic of a spin-gapped behavior. The lowest temperature region (below about 10 K) was characterized by an increase in the χ values due to the presence of impurities or defects.

In the whole range of temperatures of 1.8−300 K, the $\chi(T)$ data were fitted by the model

$$\chi(T) = \chi_0 + C_{imp}/(T - \theta_{imp}) + \chi_{spin}(T) \quad (3)$$

where χ_0 is the temperature-independent term, C_{imp} is an impurity Curie constant, and θ_{imp} is an impurity Weiss constant. For the SQSC model,[43] the $\chi_{spin}(T)$ term is given by

$$\chi_{spin}(T) = \chi_{square-tetramer}(T) = \frac{Ng^2\mu_B{}^2}{2k_BT} \frac{2 + \exp(J/k_BT) + 5\exp(-J/k_BT)}{7 + 3\exp(J/k_BT) + 5\exp(-J/k_BT) + \exp(2J/k_BT)} \quad (4)$$

The fitted parameters are g = 2.062(4) and J/k_B = 138.0(2) K, and the fitting curve is shown in Figure 6.

The value of a spin gap Δ can be estimated independently of the spin−lattice model by fitting the χ vs T data at low temperatures (i.e., eq 3 below 50 K) with the expression[1]

$$\chi_{spin}(T) = AT^{-n}\exp(-\Delta/k_BT) \quad (5)$$

The refined n value [1.023(6)] was very close to 1. Therefore, the n value was fixed at 1 during the final fitting [n = 1 and Δ/k_B = 138.9(2) K]. The obtained n value is consistent with the low-temperature limit of the spin susceptibility for a cluster (dimer) model.[1] On the other hand, for 1D $S = {}^1/_2$ Heisenberg spin systems with a spin gap, the n value should be 0.5.[1] Therefore, the results of the fitting by eqs 3 and 5 show that the spin gap of Cu_2PO_4OH arises from the presence of magnetic clusters. The J value from eq 4 is very close to the Δ value from eq 5. This supports the use of the SQSC model for Cu_2PO_4OH, for which the excitation energy (or

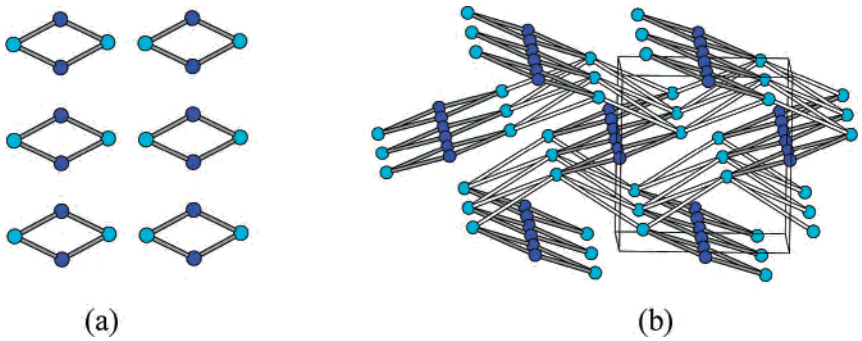

Figure 5. Schematic representations of (a) the isolated SQSCs defined by J_1 and (b) the arrangement of the SQSCs and their interactions via J_2. The gray and white cylinders represent the J_1 and J_2 paths, respectively.

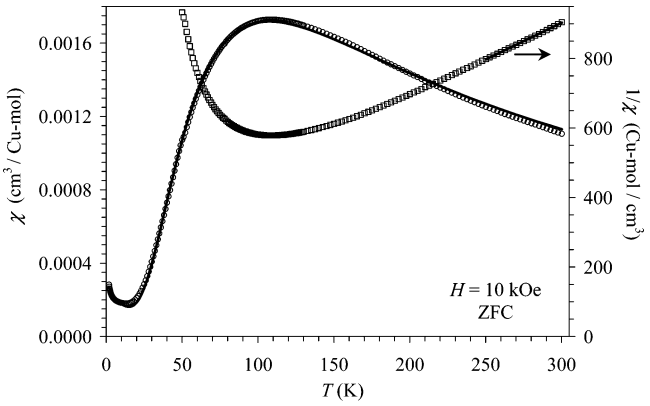

Figure 6. $\chi(T)$ and $\chi^{-1}(T)$ curves for Cu_2PO_4OH (symbols). The bold solid line on the $\chi^{-1}(T)$ curve is the fit to eq 2 at 250−300 K. The bold solid line for the $\chi(T)$ curve is the fit using the SQSC model (eqs 3 and 4) in the 1.8−300 K region.

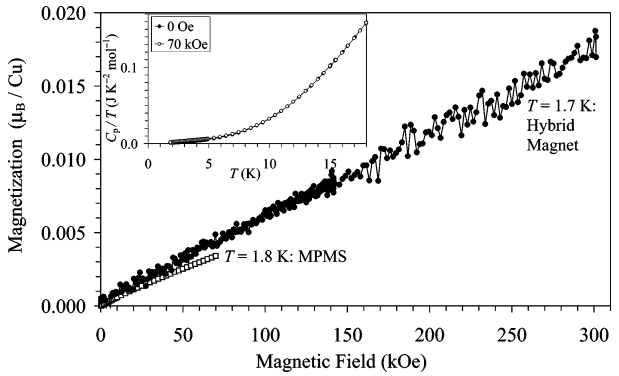

Figure 7. Isothermal magnetization curves of Cu_2PO_4OH at 1.7 K up to 300 kOe and at 1.8 K up to 70 kOe. The curves measured with an MPMS at 1.8 and 4.2 K are indistinguishable on this figure. The inset shows the C_p/T vs T curve of Cu_2PO_4OH between 1.8 and 18 K measured at 0 and 70 kOe.

the spin gap, Δ) from the $S = 0$ ground state to the $S = 1$ first excited state is J.

High-field isothermal magnetization data, M vs H, at 1.7 K show a linear increase of magnetization from 0 to 300 kOe with a magnetization value of about 0.018 μ_B per Cu^{2+} ion at 300 kOe (Figure 7). The absolute values at 70 kOe were slightly different for the measurements using the hybrid magnet and MPMS. The linear increase up to 300 kOe can be explained by difficulties in the correct subtraction of contributions from the sample holder and an Apeazon grease used to prevent the sample movement. The measurements with MPMS show a small deviation from the linear behavior, that is, two contributions. The first contribution in the magnetization (having a tendency to saturate at high magnetic fields) is due most probably to the presence of paramagnetic impurities or structural defects. The second or linear contribution in the magnetization may be attributed to the orbital susceptibility (Van Vleck term).[2] Note that a very similar M vs H curve demonstrating almost linear dependence was observed in MgV_2O_5 having a spin-singlet ground state.[2] When $J/k_B = 138$ K estimated from the susceptibility data is applied and the equation

$$\Delta/k_B = 0.6714gH \quad (6)$$

is used, it is expected that the spin-singlet ground state in Cu_2PO_4OH will be broken above 970 kOe. This value of the magnetic field is difficult to achieve in a laboratory. Inelastic neutron diffraction will be needed to probe the spin-gap value and magnetic excitations of Cu_2PO_4OH.

The specific heat data exhibit no anomaly characteristic of a long-range ordering (the inset in Figure 7), and hence this is evidence that Cu_2PO_4OH does not undergo long-range magnetic transitions down to 1.8 K. This fact is in accordance with a spin-singlet ground state of Cu_2PO_4OH. In addition, the C_p/T values approach zero at the lowest temperatures, indicating the absence of the linear term in the specific heat that would be expected for the uniform $S = {}^1/_2$ Heisenberg chain.[1]

The magnetic properties of isostructural Cu_2PO_4OH and Co_2PO_4OH are quite different. Cu_2PO_4OH has a spin-singlet ground state and no long-range ordering, while Co_2PO_4OH exhibits a long-range antiferromagnetic ordering at $T_N = 75$ K.[29] Such a difference is observed in the isostructural compounds $BaCuP_2O_7$, $BaCoP_2O_7$, and $BaNiP_2O_7$[44] and also in the isostructural compounds $Na_2Cu_2TeO_6$, $Na_2Co_2TeO_6$, and $Na_2Ni_2TeO_6$.[5,45] It is noted that the magnetic orbital of a Cu^{2+} site (usually the $x^2 - y^2$ orbital) is highly anisotropic and the spin-${}^1/_2$ Cu^{2+} ion has a strong quantum effect.

4. Concluding Remarks

Our study shows that Cu_2PO_4OH is a spin-gap system and that the spin-exchange interactions between the Cu^{2+} ions of Cu_2PO_4OH are weak within the $Cu2_2O_6(OH)_2$ dimers and within the $[Cu1_2O_6(OH)_2]_\infty$ chains but are strong between the dimers and the chains. The strongest spin-exchange interactions give rise to a weakly interacting SQSC model. The magnetic susceptibility of Cu_2PO_4OH is well described by an isolated SQSC model with one spin-exchange parameter $J/k_B = 138$ K, and the spin gap of Cu_2PO_4OH is quite close to J, in strong support of the isolated SQSC model used for Cu_2PO_4OH. Specific heat measurements show that Cu_2PO_4OH does not undergo a long-range magnetic ordering down to 1.8 K.

Acknowledgment. ICYS is supported by Special Coordination Funds for Promoting Science and Technology from MEXT, Japan. M.-H.W. is thankful for the financial support by the Office of Basic Energy Sciences, Division of Materials Sciences, U.S. Department of Energy, under Grant DE-FG02-86ER45259.

Supporting Information Available: The image of the obtained Cu_2PO_4OH crystals (Figure S1), TG and DTA curves of Cu_2PO_4OH (Figure S2), Raman spectra of Cu_2PO_4OH at room temperature (Figure S3), XRD pattern of crashed single crystals of Cu_2PO_4OH (Figure S4), magnetization curves of Cu_2PO_4OH (Figure S5), specific heat of Cu_2PO_4OH between 1.8 and 100 K (Figure S6), details of the crystal structure refinement (CIF file), and the parameters used in the EHTB calculations (Table S1). This material is available free of charge via the Internet at http://pubs.acs.org.

IC7008418

(43) Papadopoulos, A. N.; Tangoulis, A.; Raptopoulou, C. P.; Terzis, A.; Kessissoglou, D. P. *Inorg. Chem.* **1996**, *35*, 559.
(44) Belik, A. A.; Azuma, M.; Takano, M. *Inorg. Chem.* **2005**, *44*, 7523.
(45) Miura, Y.; Hirai, R.; Kobayashi, Y.; Sato, M. *J. Phys. Soc. Jpn.* **2006**, *75*, 084707.